ClinicSearch

Clinical Research and Studies

Khodayar Gholivand *

Open Access

Research Article

Graphene Oxide Functionalized with Phosphoramide as An Effective and Reliable Electrode for Supercapacitors with High-Performance

Khodayar Gholivand [1]*, Azam Barzegari [1], Fatemeh Poursalehi [2]

[1]Department of Chemistry, Faculty of Sciences, Tarbiat Modares University, Tehran, Iran.

[2]Department of Chemistry, Faculty of Sciences, Amirkabir University of Technology, Tehran Polytechnic, Tehran, Iran.

***Correspondence Author:** Khodayar Gholivand, Department of Chemistry, Faculty of Sciences, Tarbiat Modares University, Tehran, Iran.

Received Date: July 01 2025; **Accepted date:** July 10, 2025; **Published date:** July 23, 2025

Citation: Khodayar Gholivand, Azam Barzegari, Fatemeh Poursalehi, (2025), Graphene Oxide Functionalized with Phosphoramide as An Effective and Reliable Electrode for Supercapacitors with High-Performance, *Clinical Research and Studies*, 4(4); **DOI:**10.31579/2835-2882/089

Abstract

Spontaneous regression of a malignant tumor is the phenomenon of disappearance of cancer cells without any treatment. Spontaneous regression of a malignant tumor is associated with the mechanisms of apoptosis (the natural process of self-destruction of cells); immune system reactions; the impact of the tumor microenvironment; genetic factors, such as epigenetic modifications of oncogenes, tumor suppressors; hormonal reactions; the actions of various cellular proteins: cytokines, growth factors. The article discusses the process of spontaneous initiation of regression of a malignant tumor in the process of regulation by the balance of antitumor and inflammatory signals. Spontaneous regression of a malignant tumor is activated in clinical conditions that enhance the body's immune response and increase its ability to recognize and destroy cancer cells. This requires fine-tuning of the immune system. Correct enhancement of the immune response and increase in the body's ability to recognize and destroy cancer cells during spontaneous regression of malignant tumors establishes lymphocytic and plasmatic infiltration of dying tumor tissue and its environment. Studying data on spontaneous regression of cancer cells provides valuable information that can be used to improve treatment approaches. Identifying the mechanism that triggers spontaneous regression of cancer tumors will allow them to be destroyed promptly.

Key words: genetic factors; oncogenes; tumor suppressors; hormonal reactions

1.Introduction

Graphene is a singular layer of two-dimensional nanostructured sp2 carbon material that has attracted significant research in a variety of applications including, sensors 1, polymer composites 2, nanoelectronics 3, and energy storage as supercapacitors and various batteries 4, 5. The material possesses a high aspect ratio, exhibits exceptional electrical conductivity, and demonstrates favorable mechanical properties that appear to be the most alluring for supercapacitors right now. For supercapacitors, other graphene-based materials were also created, including a symmetric supercapacitor with a predetermined capacitance using chemically reduced graphene oxide 6, thermal reduction of GO to create a supercapacitor processing a specific capacitance of 132 F g -1 in a 1 M H2SO4 electrolyte 7 and GO films that have undergone electrochemical reduction have a specific capacitance of 128 F g -1 in 1 M NaNO3 8. Numerous techniques have been developed to create graphene to accomplish practical uses, most notably the arc discharge method 9, Chemical exfoliation, as well as chemical vapor deposition (CVD), and micromechanical fragmentation of highly oriented pyrolytic graphite (HOPG) 10. Liquid-phase exfoliation is one of them and is thought to be the most efficient approach for producing graphene on a wide scale and at a reasonable cost 11. GO may be chemically reduced to graphene using hydrazine or other reductants. It has also been discovered that supercapacitors with electrodes based on both graphene and graphene oxide exhibit high cyclic charge-discharge cycle life 12.

Much research has recently been undertaken to insert heteroatoms through the graphene scaffolding to create a bang gap by modulating an electron acceptor or a donor of electron characteristics, enhancing the capacitance and cycle stability in supercapacitors due to the low conductivity and inherent capacitance of graphene 13. To examine its capacitive performance, graphene has been doped with a variety of heteroatoms, including boron, nitrogen, oxygen, sulfur, and phosphor as well as their mixtures 14, 15. In their study, Yu et al. investigated the synthesis of graphene doped with X (where X represents either hydrogen (H2), iodine (I2), or bromine (Br2)) using the procedure of ball milling graphite with the addition of I2, Br2, and H2. The final product's specific capacitance and cycle ability were then assessed to determine whether or not it could be used as a supercapacitor electrode 21, all the X-doped graphene exhibits good electrochemical performance. Nitrogen-doped graphene has garnered the greatest interest within the dopants because, in addition to raising the charge carrier density, the N doping configuration results in a large interface capacitance, which is

crucial for designing the electrode material of the supercapacitor. 16, 17. Nevertheless, the surface area is drastically reduced by agglomeration brought on by intense p-p contact, which lowers capacitance 18, 19. The catalytic activity of graphene can be enhanced by doping sulfur to the carbon cage; numerous studies have shown increased activity and performance in this regard. Doping sulfur with carbon results in a positive charge shift on nearby carbon. In general, doping nitrogen is recommended for modifying the electrical characteristics of carbon materials. However, because of the huge size of the sulfur, electron pairs that make up the doped sulfur are easily polarized and exhibit increased chemical activity 20, 21.

All graphene materials doped with X (X= heteroatoms as Cl, S, N, …) exhibit exceptional electrochemical performance due to their specific capacitance and prolonged stability. Nevertheless, it has been demonstrated that chlorine-doped graphene oxide increases capacity well, and high specific capacity has been reached because of the high degree of structural defects. 12, 22. Based on our comprehensive review of existing literature, it appears that the potential use of phosphoramide-functionalized graphene oxide (L-GO) in supercapacitor applications has not been thoroughly investigated. The using of all N, P, and S dopants in the massive ligand of phosphoramide which also can prevent agglomeration of graphene oxide is noticeable. Hence, it is anticipated that these phosphoramide-functionalized graphene oxide materials have significant promise to be used as electrode materials for supercapacitors. Based on the aforementioned reasons we first doped GO with Cl as its good performance and then substituted it with phosphoramide and compared them with each other.

This work presents the methodology employed for the synthesis of chlorine-doped graphene oxide (Cl-GO) and phosphoramide bis (5-amino-1,3,4-thiadiazol-2-yl) phenylphosphonotrithioate-funcltionalized graphene oxide (L-GO) using GO that has been firstly doped by Cl and then functionalized with L ligand, respectively. Herein, we introduced L in chloroform and triethylamine dropwise to dispersed Cl-GO and refluxed to synthesize the chlorine-doped graphene oxide (Cl-GO) functionalized with L ligand (L-GO) with enhanced capacitive performance. Due to the leaving group of Cl during the process of converting graphene oxide to L-GO, phosphoramide (L) is at the same time functionalized into the carbon scaffold in substitution with Cl. The incorporation of phosphoramide ligands into the graphene framework results in a significant enhancement of the surface area that is available for ions and electron mobility. This improvement in electrical has the potential to widely progress the internal resistance of the L-GO when used as electrode material. The L-GO electrode, with a bulk weight of 1.5 mg cm-2, exhibits a notable increase in electrochemical performance. This results in a specific capacitance (Cg) of 206.8 F g -1 at the current density of 1A g -1. Furthermore, the L-GO material represents a great capacitance retention of 72.6% under a higher current density of 50 A g -1, providing a specific capacitance of 150.1 Figure -1.

2. Experimental

2.1. Materials

5-Amino-1,3,4-thiadiazole-2-thiol (C3H5N3S2, with a stated purity 95%), phenylphosphonothioic dichloride (C6H5Cl2PS, with a stated purity 97%), triethylamine ((C2H5)3N, 99%), graphite flakes, potassium permanganate ($KMnO_4$), hydrogen peroxide (H2O2, 90%), hydrochloric acid (HCl, 37%), sulfuric acid (H2SO4, 98%), acetonitrile (anhydrous, 99.8%), sodium nitrate (NaNO3, 99%), ethanol (C2H5OH, 98%), thionyl chloride (SOCl2, 99%), tetrahydrofuran (THF, C4H8O, 99.8%), dimethyl formamide (DMF, C3H7NO, 99.98%), dichloromethane (DCM, CH2Cl2, 99%), and chloroform was taken from Sigma-Aldrich and consumed without extra purification.

2.2. Preparation of GO

GO was prepared by modification of Hummers' method by oxidizing purified graphite and described elsewhere 23, 24. The graphite sheets (2g) and $NaNO_3$ (1 g) were placed into H2SO4 (140 ml) solution and stirred at a temperature of 0 °C for half an hour. Afterward, KMnO4 (6 g) was introduced drop by drop to the above-mentioned solution, and stirring continued for 4 h. The resultant mixture in the water bath was then stirred for 3 hours at the temperature of 35 °C until changed to a brown paste, 200 ml of deionized water (DI) was introduced gently and stirred at the temperature of 90 °C for 30 minutes. Then, H2O2 was added dropwise to the mixture and continued until gas production stopped. The obtained yellow mixture was refined and purified with DI and HCl (1 M) at various times until pH was neutralized. The synthesized GO was dried at the temperature of 45 ◦C.

2.3. Preparation of Cl-GO

Replacement of the hydroxyl groups (OH) of GO with Cl was executed by thionyl chloride (SOCl2) to produce Cl-GO. 200 mg GO was dispersed in 15 ml SOCl2 for 1 hour and refluxed at 70 ◦C for 24 hours in DMF. The pure Cl-GO was obtained after washing with THF, DMF, and DCM.

2.4. Synthesis of L

To synthesize L, 1 mmol related phenylphosphonothioic dichloride was dropwise added to the 1.1 mmol of 5-Amino-1,3,4-thiadiazole-2-thiol and triethylamine in acetonitrile at 0 °C, and stirred for 24 hours and then dried at room temperature. The white obtained powder was washed with deionized water to emit triethylammonium salt 25.

2.5. Synthesis of L-GO

The mixture of 0.4 g L in chloroform and triethylamine was introduced drop by drop to dispersed Cl-GO and refluxed at 50 ◦C for 72 hours. After that, the mixture was eluted with dichloromethane and ethanol to eliminate by-products. The product dried at the temperature of 50 ◦C to generate L-GO (Scheme 1).

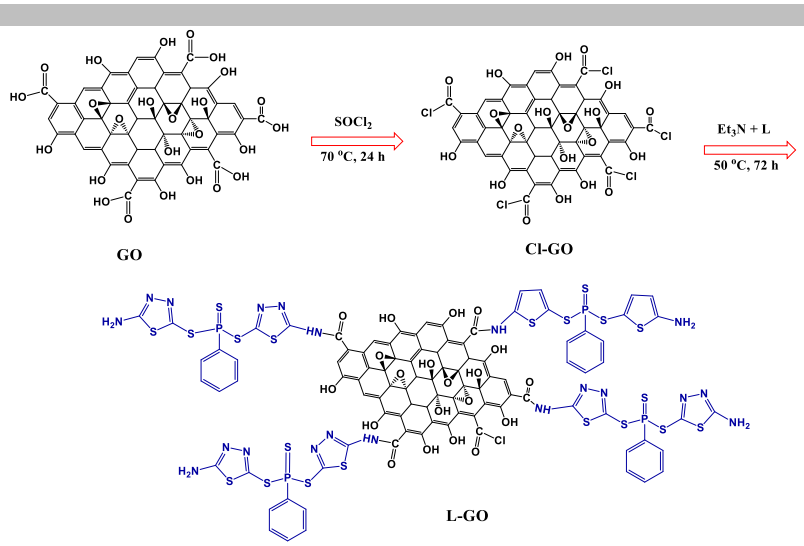

Scheme 1: Illustration of the Preparation procedure of Cl-GO and L-GO.

2.6. Characterizations

X-ray diffraction (XRD) examinations of synthesized GO, Cl-GO, and L-GO were examined with a system (X'Pert MPD) equipped with a sealed Cu Kα radiation source (λ = 1.54060 Å). The angular range of ω=5° to ω=89.9° set at a scan rate of 0.1° min-1.

Fourier Transform Infrared Spectroscopy (FT-IR) spectra were recorded on a Shimadzu model IR-60 spectrometer using KBr pellets. SEM (FEI ESEM QUANTA 200, USA) and EDX (EDS Silicon Drift 2017, USA) were utilized. The accelerating voltage of SEM-EDX was 10 kV, and all samples were treated with gold spray for 1 min in a vacuum.

2.7. Electrode preparation and electrochemical measurements

The electrochemical performance of electrodes was figured out using cyclic voltammetry (CV), galvanostatic charge/discharge (GCD), and electrochemical impedance spectroscopy (EIS). The tests were carried out in a three-electrode setup with a platinum rod serving as the reference electrode and an Ag/AgCl (3.0 M KCl) electrode serving as the counter electrode, respectively. The PGSTAT 302N Autolab instrument was used for electrochemical tests. To create the working electrode, a slurry mixture of active compound powder (Cl-GO or L-GO), carbon black, and PVDF with the %wt. ratio of 80:10:10 was applied onto the surface of Ni foam. NMP was used as the solvent of the slurry. The L-GO and Cl-GO-coated Ni foam were dried at 80 ºC for 12 hours. A 3 M KOH solution in water served as the supporting electrolyte. The CV tests covered a potential range of 0 V to 1 V compared to Ag/AgCl, at the scan rate of 10 mV s -1 to 50 mV s -1. GCDs were conducted at a current density of 1 A g -1 to 50 A g -1, within the potential window of 0 to 1 V compared to Ag/AgCl.

We used the EIS approach in the frequency window of 100 kHz to 100 MHz with an amplitude of 10 mV to measure the electronic resistance and capacitive behavior of the active compounds. Using the NOVA 1.11 program, the appropriate equivalent circuit was fitted for the EIS plots. Every electrochemical experiment was carried out at 25 °C, the average room temperature.

3. Result and discussion

3.1. Characterization of GO, Cl-GO, and L-GO

XRD was carried out as a phase verification of the crystallized products. Fig. 1 displays the XRD diffraction patterns of GO, Cl-GO, and L-GO powders. The strong and sharp diffraction peak in Fig.1(a) at 2θ = 10.09◦ ascribed to the C(001) peak corresponds to a graphene layer that has a d-spacing of 0.87 nm indicating the oxidation of graphite 15, 26. From a comparison of Fig. 1(a) and Fig. 1(b), it can be realized the difference in the XRD patterns of GO and Cl-GO. The doping of graphene oxide with chlorine results in a structural change that is confirmed by the comparison of the XRD pattern of GO and Cl-GO. The X-ray diffraction pattern of Cl-GO shows a sharp peak at 2θ =23.12˚ attributed to the C(002) peak indicating almost all oxygen groups in the Cl-GO 27 have been removed. Fig. 1(c) depicts the XRD pattern of L-GO which shows the sharp peak at 2θ = 24.59◦ ascribed to the C (002) peak. However, the diffraction peak of C(002) related to L-GO is broad, and its intensity is low in comparison with Cl-GO, which suggests the decreased stacked graphene sheets originated from the presence of massive phosphoramide molecules between graphene sheets 28.

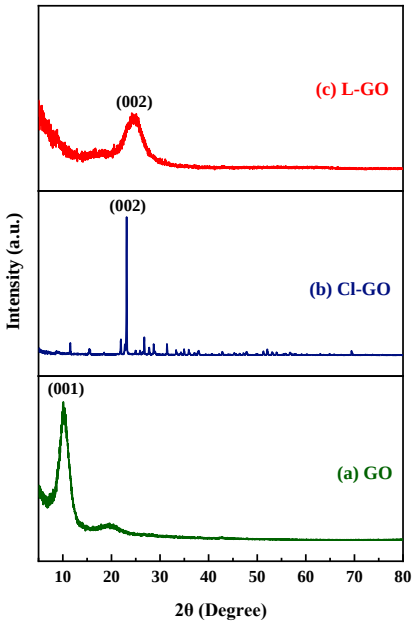

Figure 1: XRD patterns of GO (a), Cl-GO (b), and L-GO (c).

Figure 2 shows the FT-IR spectrum of GO, Cl-GO, and L-GO. The spectrum of GO has been represented in Figure. 2 (a); broad peaks of 3432 cm-1 correspond to the –OH group. The peaks at 1716 cm-1, 1627 cm-1, and 1054 cm-1 originated from the vibration of the C=O, C=C, and C-O-C functional groups. Figure. 2 (b) displays that after Cl-doped into graphene, the intensity of peaks related to carboxylic acid groups decreased. The difference in the number of functional groups has reduced the intensity of the peak OH in Cl-GO and confirms the replacement of OH with Cl 29. When modifying Cl-GO with phosphoramide, new peaks can be observed in Figure. 2 (C). The bands at 1194 cm-1 and 1127 cm-1 indicate P–O and P=O bonds exist in L-GO. Furthermore, the peak at 1716 cm-1 absconded in L-GO.

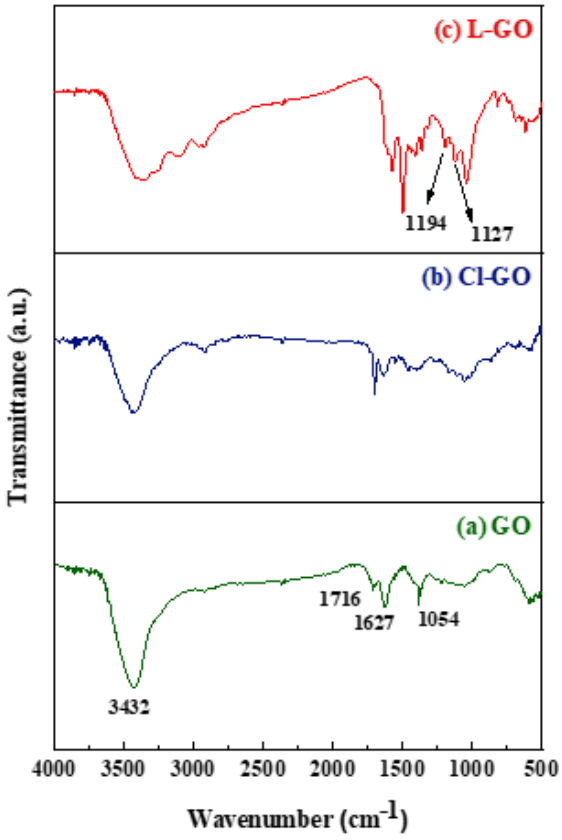

Figure 2: FT-IR of GO (a), Cl-GO (b), and L-GO (c).

The morphology and elemental analysis of the prepared GO, Cl-GO, and L-GO were investigated using SEM, EDAX, and mapping. Figure. 3 presents the SEM images of the (a) GO, Cl-GO (b), and (c) L-GO. As can be seen, the structure of GO is layered. Hydrogen bonding of the oxygen-containing

functional groups caused the wrinkly morphology of GO sheets. The wrinkle-like structure also can be observed on the surface and the edge of Cl-GO. The rougher surface of Cl-GO in comparison with GO surface and many apparent cracks were detected due to the Cl-doping into GO sheets. After modification of Cl-GO with phosphoramide, the changing of structure and morphology of L-GO is clear compared with Cl-GO. So, apparent changes in the morphology of L-GO confirmed the attachment of massive L ligands on Cl-GO layers 30.

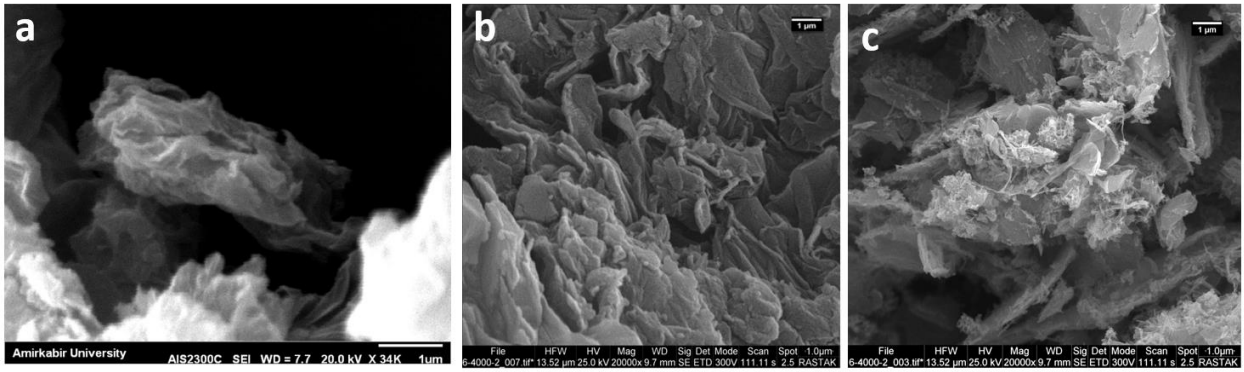

Figure 3: SEM images of GO (a), Cl-GO (b), and L-GO (c).

Figure. 4 (a) shows the elemental mapping of L-GO. The elements of nitrogen, oxygen, phosphorus, and sulfur are uniformly distributed throughout the L-GO. Figure. 4 (b), the EDAX for the L-GO illustrated the peaks corresponding P, N, O, and S which have the weight percentage of 18.82%, 24.81%, 2.14%, and 17.01%, which confirmed the presence of phosphoramide in L-GO layers.

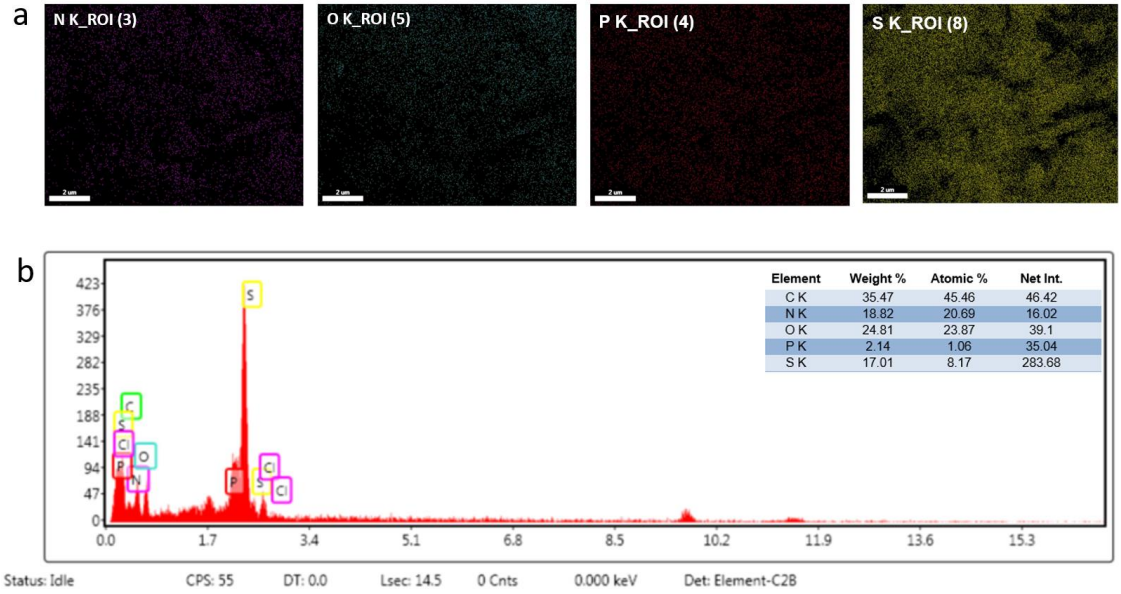

Figure 4: Corresponding elemental maps (a), EDAX analyses of L-GO (b).

3.2. Electrochemical Properties of the Supercapacitors (Cl-GO and L-GO)

Ni foam, Cl-GO, and L-GO samples were analyzed in a 3.0 M KCl aqueous solution to evaluate the specific capacitance of different electrodes. The potential is applied in the range of 0 to 1 V at a scan rate of 50 mV s -1. As shown in Figure. 5; the bare Ni foam electrode did not significantly contribute to the charge storage process in 3.0 M KCl. The CV curves for the Cl-GO and L-GO electrodes based on Ni foam indicate an electrochemical capacitor, with an approximately rectangular feature observed in the potential intervals beyond 0.6 V. The difference in specific capacitance is possible to calculate by comparison of the area under the cyclic voltammetry (CV) curve in a defined voltage window. The specific capacitance of layered graphene oxide (L-GO) is greater in comparison to chlorine-doped graphene oxide (Cl-GO). The presence of residual oxygen groups attached to carbonyl groups on the surface of Cl-GO and L-GO sheets gives rise to redox peaks and pseudocapacitive properties. These phenomena are a result of both faradaic and non-faradaic processes 31.

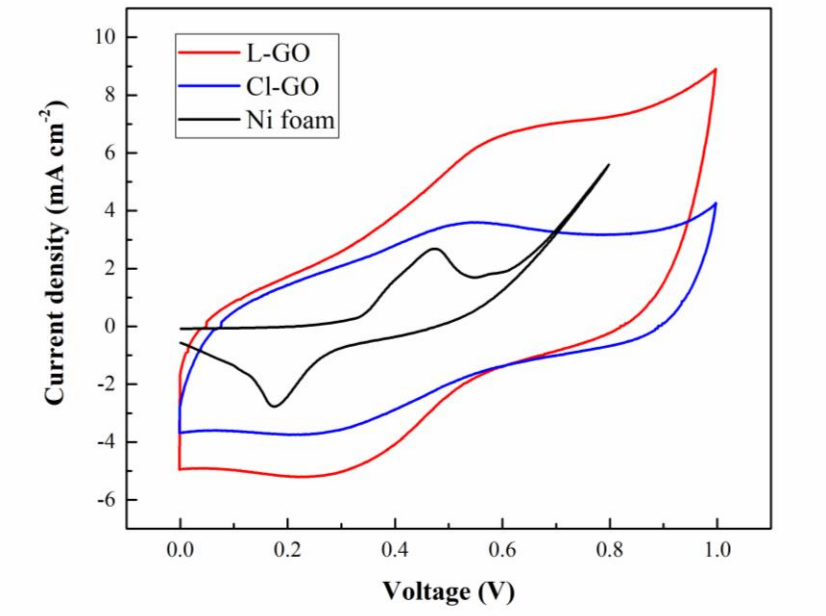

Figure 5: CV curves at 50 mVs-1 for Ni foam, Cl-GO, and L-GO.

Figure 6 illustrates the fluctuation in specific capacitance of chlorine-doped graphene oxide (Cl-GO) and phosphoramide-induced graphene oxide (L-GO) electrodes in different scan rates. Upon examination of the cyclic voltammetry (CV) profiles of Cl-GO and L-GO, it was noted that the specific capacitance exhibited a decline with the escalation of scan rates ranging from 10 to 50 mV s-1. Both capacitors demonstrated a broad redox wave ranging from 0 to 0.6 V, followed by a rectangular form at potentials beyond 0.6 V. This observation indicates the presence of both pseudocapacitance and electrical double-layer capacitance. At comparable scan rates, the specific capacitance of the L-GO electrode represents a distinguished value when compared to the Cl-GO, and the reason for that can be related to the presence of phosphoramide ligand and especially the presence of NH2 and SO2 groups in it.

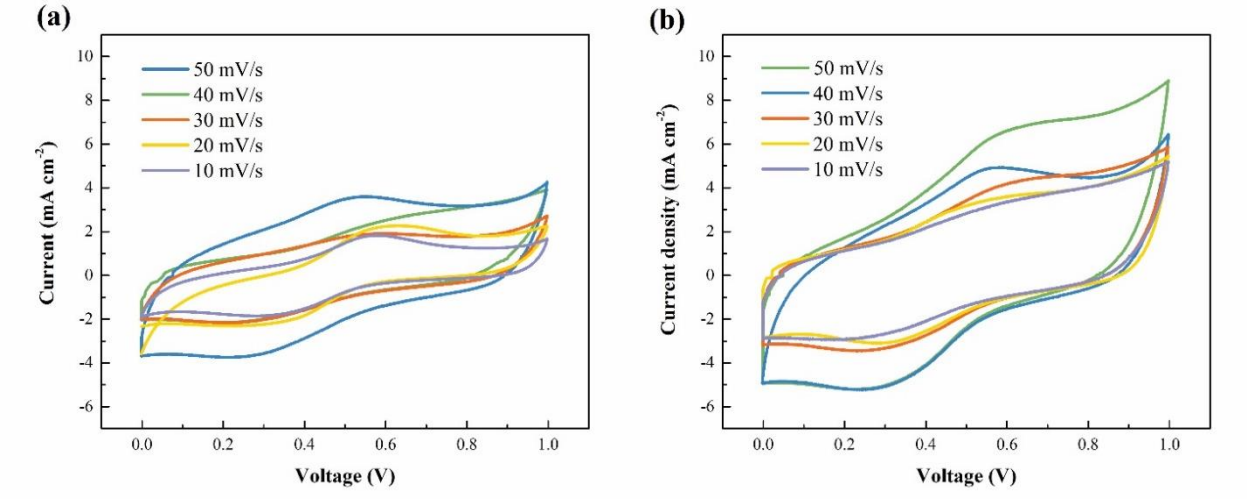

Figure 6: CV curves of (a) Cl-GO, and (b) L-GO at different scan rates.

The galvanostatic charge/discharge (GCD) curves are indicated to distinguish the electrochemical capacitance of Cl-GO and L-GO at current densities of 1 and 50 A g -1 in Figure. 7. GCD curves of Cl-GO and L-GO electrodes show symmetric and quasi-triangular form without obvious IR drop at 1 A g -1, which confirms ion transportation and fast charge transferring. As current densities decline from 1 to 50 A g-1, the period of charge and discharge decreases, and IR drop increases to about 0.5 and 0.4 V for Cl-GO and L-GO, respectively. The lower IR drop for L-GO confirms its lower internal resistance because of the π-donor phosphoramide ligand. In addition, L-GO has a higher charge-discharge duration compared to Cl-GO, because of high electron mobility and ion-accessible surface area certifying efficient capacitive performance. As expected, this consequence follows those from the CV measurements 32.

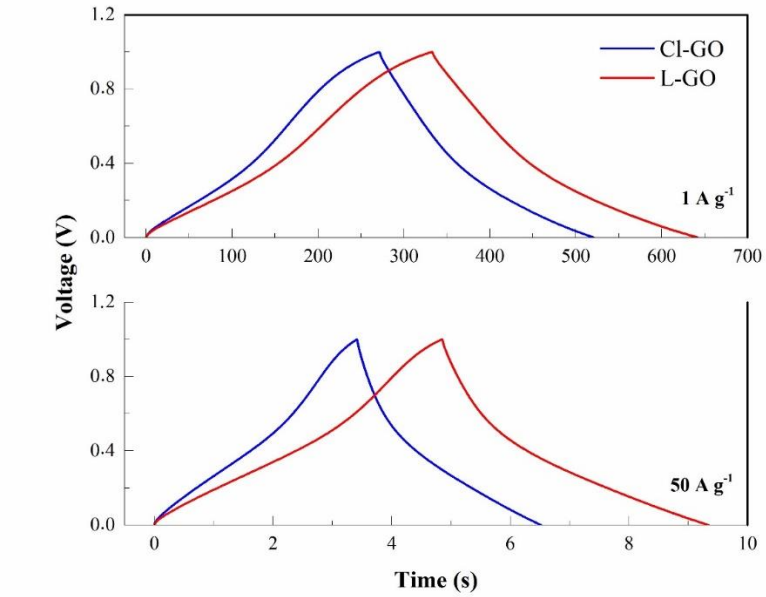

Figure 7: GCD curves of Cl-GO and L-GO at 1 and 50 A g -1.

The specific capacitance (C) is determined by analyzing the galvanostatic charge-discharge (GCD) curves and is expressed in units of Farads per gram (F g -1). to Eq. 1.

$$Cs = \frac{It}{m\Delta V} \qquad \text{Equation (1)}$$

The formula for calculating discharge current (A) takes into account the discharge time (s), the mass of active material (g), and the potential range (V) 33, 34.

The correlation between Cg and current density is shown in Fig. 8. When tested at a rate of 1 A g -1, L-GO exhibits a remarkably great Cg of 206.8 F g -1. This is a significant increase of 24.3% compared to Cl-GO, which only achieves a Cg of 166.3 F g -1. It appears that L-GO has better rate capability compared to Cl-GO, as even at 50 A g -1 current density, its Cg remains at 72.7% (150.1 F g -1), which is significantly greater than Cl-GO 62.3% (103.6 F g -1). In addition, L-GO exhibits a significant specific volume capacitance (Cv) of 310.2 mF cm -2 at 1 A g -1. The greater specific capacitance and impressive capacitive performance exhibited by increased electron mobility and ion-accessible surface area can be explained by the L functionalizing graphene oxide-based electrode. Table 1 represents the graphene oxide functionalized with phosphoramide (L-GO) in this work with other heteroatom-doped graphene oxide in similar articles. As can be seen, in comparison to some previous works, the L-GO in the present work has improved the specific capacitance and competed with the others.

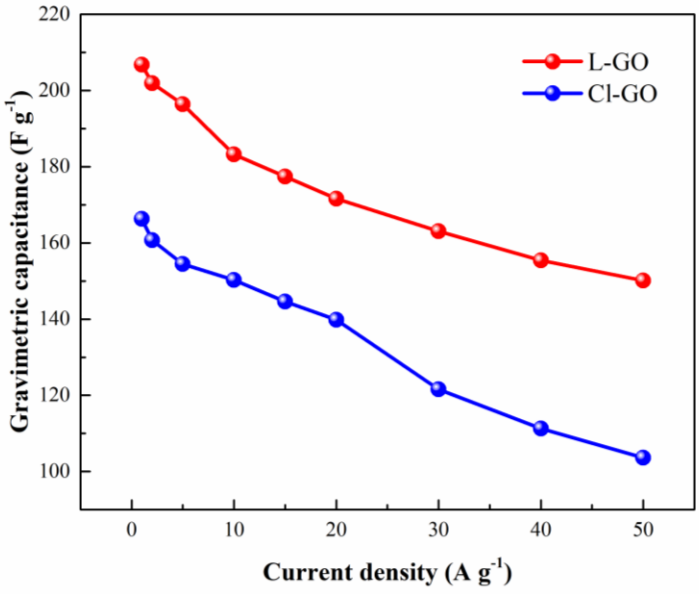

Figure 8: Cg of L-GO and Cl-GO at different current densities.

Electrode	Hetroatom doped	Specific capacitance (F g $^{-1}$)	Reference
Cl-RGO	Cl	210 at 1 A g^{-1}	[38]
S-GO	S	206.4 mF/cm^2 at 10 mA cm^{-2}	[39]
N-GO	N	533.2 mF/cm^2 at 10 mA cm^{-2}	
Cl-GO	Cl	1098 mF/cm^2 at 10 mA cm^{-2}	
Cl-RGO	Cl	178.4 at 1 A g^{-1}	[40]
N-RGO	N	111.3 at 0.2 A g^{-1}	[41]
B-RGO	B	82.9 at 0.5 A g^{-1}	
B/N-RGO	B/N	130.7 at 0.2 A g^{-1}	
P-RGO	P	115 at 0.05 A g^{-1}	
S-RGO	S	343 at 0.2 A g^{-1}	
S/N-RGO	S/N	264.3 at 0.5 A g^{-1}	[42]
B-RGO	B	-	[43]
N-RGO	N		
S-GO	S	211 at 1 A g^{-1}	[44]
S-RGO	S	320 at 3 A g^{-1}	[45]
N-RGO	N	96.4 at 0.1 A g^{-1}	[46]
L-GO	Phosphoramide	206.8 at 1 A g^{-1} 310.2 mF/cm^2 at 1.5 mA cm^{-2}	This work

Table 1: Comparison of the results of this work with previous similar articles.

The Cl-GO and L-GO electrodes underwent electrochemical impedance spectroscopy (EIS) measurements at open circuit voltage, with an AC perturbation of 10 mV, in the frequency range of 100 kHz to 100 MHz (Fig. 9). These measurements were conducted previous to the 1st cycle. The impedance spectra exhibit a notable resemblance in their form, characterized by the presence of a semicircular pattern at frequencies ranging from high to medium, as well as a linear trend at low frequencies. This similarity persists in both of the analyzed samples. In electrochemical analysis, the semicircle appearing at high frequency indicates charge-transfer resistance caused by the inherent resistivity of the electrode material 35. On the other hand, the straight line observed is associated with the bulk diffusion resistance of the material. The charge transfer resistance for Cl-GO experiences about 5 Ω 36. The L-GO electrode shows a decline in charge transfer resistance of about 5 Ω (for Cl-GO) to 2 Ω, respectively. The Rct amounts are lower for L-GO electrodes because of the high electrical conductivity originating from π-donor groups of phosphoramide in L-GO. The Warburg resistance, which can be observed through the displacement in the direction of the x-axis perceived at the endpoint of the semicircular segment of the Nyquist curve, is also enhanced. Compared to Cl-GO, the L-GO electrode exhibits a more vertical line at low frequencies, signifying a superior capacitive process and less resistance to ion diffusion 37.

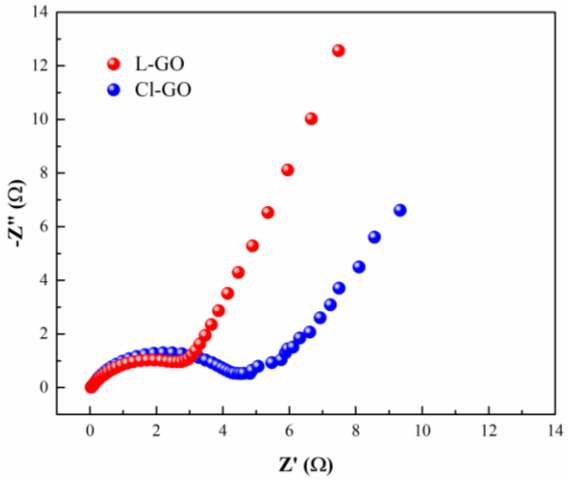

Figure 9: Nyquist plots of Cl-GO, and L-GO.

4. Conclusion

In summary, electrode materials for supercapacitors were generated by functionalizing the edges of graphene oxide (GO) using ligand (L), which was introduced dropwise to chlorine-doped graphene oxide (Cl-GO) and refluxed. The existence of Cl in GO and phosphoramide in L-GO was surveyed using X-ray diffraction (XRD), Fourier transforms infrared spectroscopy (FT-IR), field emission scanning electron microscopy (FE-SEM), and energy dispersive x-ray spectroscopy (EDX) characterization techniques. The presence of phosphoramide ligands, in addition to increasing electron agglomeration and space charge, facilitates the access of electrons to the electrode, preventing the accumulation of graphene sheets. L ligands can improve electron mobility in Cl-GO, resulting in a higher charge capacitance. In comparison to Cl-GO material with a specific capacitance of 166.3 F g -1, L-GO has a specific capacitance of 206.8 F g -1 at 1 A/g. Moreover, the specific capacitance displayed high rate capability and capacitance of 150.1 F g -1 (remaining 72.6% capacitance) even at 50 A/g. Therefore, L-GO could be used as an electrode material for high-performance supercapacitors due to its great specific capacitance and good rate capability. This tactic offers a fresh path for high-energy-density

supercapacitors, which hold promise as a potential source of energy in the future.

References

1. Huang, H.; Su, S.; Wu, N.; Wan, H.; Wan, S.; et al. (2019). Graphene-based sensors for human health monitoring. *Frontiers in chemistry* 7, 399.
2. Díez-Pascual, A. M.; Rahdar, A., (2022). Graphene-based polymer composites for flexible electronic applications. Micromachines 13 (7), 1123.
3. Radsar, T.; Khalesi, H.; Ghods, V., (2021), Graphene properties and applications in nanoelectronic. Optical and Quantum Electronics 53, 1-38.
4. Zhang, Y.; Xia, X.; Liu, B.; Deng, S.; Xie, D.; et al.,(2019). Multiscale graphene-based materials for applications in sodium ion batteries. Advanced Energy Materials 9 (8), 1803342.
5. Velasco, A.; Ryu, Y. K.; Boscá, A.; Ladrón-de-Guevara, A.; Hunt, E.; et al., (2021). Recent trends in graphene supercapacitors: from large area to microsupercapacitors. Sustainable Energy & Fuels 5 (5), 1235-1254.
6. Stoller, M.; Park, S.; Zhu, Y.; An, J.; Ruoff, R., (2008). Nano Lett. Nano Lett, 8, 3498.
7. Le, L. T.; Ervin, M. H.; Qiu, H.; Fuchs, B. E.; Lee, W. Y., (2011). Graphene supercapacitor electrodes fabricated by inkjet printing and thermal reduction of graphene oxide. Electrochemistry Communications 13 (4), 355-358.
8. Peng, X.-Y.; Liu, X.-X.; Diamond, D.; Lau, K. T., (2011). Synthesis of electrochemically-reduced graphene oxide film with controllable size and thickness and its use in supercapacitor. Carbon 49 (11), 3488-3496.
9. Pham, T. V.; Kim, J. G.; Jung, J. Y.; Kim, J. H.; Cho, H.; et al., (2019). High areal capacitance of N-doped graphene synthesized by arc discharge. Advanced Functional Materials 29 (48), 1905511.
10. Park, S.; Floresca, H. C.; Suh, Y.; Kim, M. J., (2010). Electron microscopy analyses of natural and highly oriented pyrolytic graphites and the mechanically exfoliated graphenes produced from them. Carbon 48 (3), 797-804.
11. Andrić, S.; Tomašević-Ilić, T.; Bošković, M. V.; Sarajlić, M.; Vasiljević-Radović, D.; et al. (2020). Ultrafast humidity sensor based on liquid phase exfoliated graphene. Nanotechnology 32 (2), 025505.
12. Arvas, M. B.; Gürsu, H.; Gencten, M.; Sahin, Y., (2021).Preparation of different heteroatom doped graphene oxide based electrodes by electrochemical method and their supercapacitor applications. *Journal of Energy Storage* 35, 102328.
13. Xu, G.; Zhao, J.; Yuan, J.; Zhao, Y.; Yin, H.; et al., (2022). A facile one-pot microwave assisted hydrothermal synthesis of hierarchical cobalt oxide/reduced graphene oxide composite electrode for high-performance supercapacitors. *Journal of Alloys and Compounds* 897, 163163.
14. Chen, W.; Ge, C.; Li, J. T.; Beckham, J. L.; Yuan, Z.; et al., (2022). Heteroatom-doped flash graphene. ACS nano 16 (4), 6646-6656.
15. Gholivand, K.; Barzegari, A.; Yousefian, M.; Malekshah, R. E.; Faraghi, M., (2023). Experimental and theoretical evaluation of biological properties of a phosphoramide functionalized graphene oxide. Biocatalysis and Agricultural Biotechnology 102612.
16. Bie, C.; Yu, H.; Cheng, B.; Ho, W.; Fan, J.; et al. (2021). Design, fabrication, and mechanism of nitrogen-doped graphene-based photocatalyst. Advanced Materials 33 (9), 2003521.
17. Zhou, J.; Xie, M.; Wu, F.; Mei, Y.; Hao, Y.; et al., (2021). Ultrathin surface coating of nitrogen-doped graphene enables stable zinc anodes for aqueous zinc-ion batteries. Advanced Materials 33 (33), 2101649.
18. You, B.; Wang, L.; Yao, L.; Yang, J., (2013). Three dimensional N-doped graphene–CNT networks for supercapacitor. Chemical communications 49 (44), 5016-5018.
19. Zhu, C.; Dong, S., (2013). Recent progress in graphene-based nanomaterials as advanced electrocatalysts towards oxygen reduction reaction. Nanoscale 5 (5), 1753-1767.
20. Kumar, N. A.; Baek, J.-B., (2015). Doped graphene supercapacitors. Nanotechnology 26 (49), 492001.
21. Gholivand, K.; Sarmadi-Babaee, L.; Faraghi, M.; Badalkhani-Khamseh, F.; Fallah, N., (2022). Heteroatom-containing phosphoramides as carbon steel corrosion inhibitors: Density functional theory and molecular dynamics simulations. Chemical Physics Impact 5, 100099.
22. Kakaei, K.; Hamidi, M.; Husseindoost, S., (2016). Chlorine-doped reduced graphene oxide nanosheets as an efficient and stable electrode for supercapacitor in acidic medium. *Journal of colloid and interface science* 479, 121-126.
23. Zaaba, N.; Foo, K.; Hashim, U.; Tan, S.; Liu, W.-W.; et al., (2017). Synthesis of graphene oxide using modified hummers method: solvent influence. Procedia engineering 184, 469-477.
24. Chen, J.; Yao, B.; Li, C.; Shi, G., (2013). An improved Hummers method for eco-friendly synthesis of graphene oxide. Carbon 64, 225-229.
25. Gholivand, K.; Barzegari, A.; Kashani, H. M.; Fallah, N., Two novel phosphoramide derivatives moiety as corrosion inhibitor for mild steel: Experimental and theoretical study. Applied Organometallic Chemistry, e7314.
26. Chen, P.; Li, H.; Song, S.; Weng, X.; He, D.; et al., Adsorption of dodecylamine hydrochloride on graphene oxide in water. Results in physics 7, 2281-2288.
27. Ju, H.-M.; Choi, S.-H.; Huh, S. H., (2010). X-ray diffraction patterns of thermally-reduced graphenes. J. Korean Phys. Soc 57 (6), 1649.
28. Yan, J.; Wei, T.; Shao, B.; Ma, F.; Fan, Z.; et al., (2010). Electrochemical properties of graphene nanosheet/carbon black composites as electrodes for supercapacitors. Carbon 48 (6), 1731-1737.
29. She, X.; Liu, T.; Wu, N.; Xu, X.; Li, J.; et al., (2013). Spectrum analysis of the reduction degree of two-step reduced graphene oxide (GO) and the polymer/r-GO composites. Materials Chemistry and Physics 143 (1), 240-246.
30. Shuang, S.; Girardi, L.; Rizzi, G. A.; Sartorel, A.; Marega, C.; et al., (2018). Visible light driven photoanodes for water oxidation based on novel r-GO/β-Cu2V2O7/TiO2 nanorods composites. Nanomaterials 8 (7), 544.
31. Zhu, T.; Li, S.; Ren, B.; Zhang, L.; Dong, L.; et al., (2019). Plasma-induced synthesis of boron and nitrogen co-doped reduced graphene oxide for super-capacitors. Journal of Materials Science 54 (13), 9632-9642.
32. Pal, R.; Goyal, S. L.; Rawal, I.; Gupta, A. K., (2021). Efficient energy storage performance of electrochemical supercapacitors based on polyaniline/graphene nanocomposite electrodes. Journal of Physics and Chemistry of Solids 154, 110057.
33. Hekmat, F.; Shahrokhian, S.; Taghavinia, N., (2018). Ultralight flexible asymmetric supercapacitors based on manganese dioxide–polyaniline nanocomposite and reduced graphene oxide electrodes directly deposited on foldable cellulose papers. *The Journal of Physical Chemistry* C 122 (48), 27156-27168.

34. Mahdi, F.; Javanbakht, M.; Shahrokhian, S., (2021). Anodic pulse electrodeposition of mesoporous manganese dioxide nanostructures for high performance supercapacitors. Journal of Alloys and Compounds 887, 161376.
35. Poursalehi, F.; Javanbakht, M.; Daryakenari, A. A.; Gao, B., (2023). Binder-Free LiNi0. 8Mn0. 1Co0. 1O2/Multi-Walled Carbon Nanotube Prepared by One-Step Electrophoretic Deposition Method for Efficient Li-Ion-Battery Cathodes. Journal of The Electrochemical Society 170 (8), 080508.
36. Yan, J.; Wei, T.; Fan, Z.; Qian, W.; Zhang, M.; et al., (2010). Preparation of graphene nanosheet/carbon nanotube/polyaniline composite as electrode material for supercapacitors. Journal of Power Sources 195 (9), 3041-3045.
37. Li, J.; Xie, H.; Li, Y.; Liu, J.; Li, Z., (2011). Electrochemical properties of graphene nanosheets/polyaniline nanofibers composites as electrode for supercapacitors. *Journal of Power Sources* 196 (24), 10775-10781.